15th IFK
Proc. of the 15th International Fluid Power Conference <Symposium/Conference>
<DOI>

Beyond Pilot Control: A Prototype for Direct Actuation of Large Industrial Proportional Valves

Author: Tobias Vonderbank[1], Prof. Katharina Schmitz[1]

[1]Institute for Fluid Power Drives and Systems(ifas), RWTH Aachen University, Aachen, Germany

Corresponding Email: tobias.vonderbank@ifas.rwth-aachen.de

Abstract.

Recent advancements in electric drive technology are enabling new applications in hydraulics, particularly in valve actuation. New electric actuators based on stepper or BLDC motors offer higher forces and virtually unlimited stroke lengths, making them viable alternatives to conventional solenoids, especially for large hydraulic valves that have traditionally required hydraulic pilot systems. These actuators have already been successfully utilized in mobile machinery, where they enable the direct actuation of large valves, resulting in a simplified system architecture and improved efficiency. However, in stationary hydraulics, direct electromechanical actuation nowadays is limited to valves of NS10 due to the high forces required. Whereby the flow and spring forces constitute the most significant share of the total actuation force. This work investigates strategies for reducing flow forces to enable direct actuation of NS16 proportional valves with the actuators mentioned before, based on electric motors. Based on theoretical analysis, design modifications on the spool and housing/sleeve for flow force reduction are identified and evaluated using CFD simulations and measurements. The resulting optimized valve design significantly reduces actuation force requirements, providing a feasible pathway for direct electromechanical actuation of larger industrial valves and eliminating the need for pilot stages.

Keywords. Pilot Controlled Valves, Direct Valve Actuation, Flow Force Reduction, Experimental, CFD-Simulation

1. INTRODUCTION

The use of stepper motors for controlling hydraulic valves in mobile machinery has been explored since the 1990s. Started when the hydraulic pilot control of a tractor's lift valve was replaced by an electromechanical actuator based on a stepper motor back in 1995 [1]. Followed by the direct actuation of the front loader valve in 2000 [2]. One of the key motivations for this research was the potential to simplify the overall system by eliminating the separate pilot-control circuit that had been necessary up to that point [2]. Additionally, other significant advantages of stepper motor-based valve actuators were emphasized, including their high rigidity and force capabilities, as well as their ability to achieve stable and precise positioning [1].

While the application of stepper motors was reported only sporadically in the 1990s and subsequent years, there has been a notable increase in activity over the last ten years regarding stepper motor-based electromechanical valve actuators. These developments have primarily been driven by the company SONCEBOZ, which has been publishing articles on the subject since 2014, presenting the latest research findings on their S42 and S40 actuators. That this research addresses market demands is evident, as Sonceboz is not the only company active in this field. For example, there was another actuator based on an electric motor presented by THOMAS MAGNETE at the 9th IFK. Both actuators the S40 by SONCEBOZ and the EMA by THOMAS MAGNETE are shown in **Figure 1**. [3]–[8]

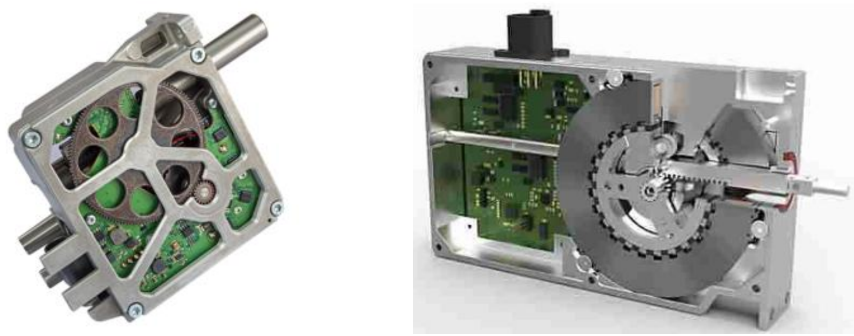

Figure 1: S40 Actuator by Sonceboz [4], [9] and EMA-Actuator by Thomas Magnete [8]

Although the discussion about motor-based valve actuators is primarily led by individual companies that are active in the field of electromechanical actuation, while focusing their research on their specific actuators to enhance performance and extend their limits further, there has also been a growing momentum in university research in recent years. In contrast to the aforementioned company-led research, university studies focus on decreasing the necessary actuation forces [10]–[17] or fundamental analyses of pilot-controlled valves aiming to optimize their performance [18]–[20].

Overall, it is evident that direct control of large valves has been increasingly discussed in research and application for about a decade, and the first market-ready actuators are now available [4]–[6]. Compared to solenoid magnets, they are characterized by higher forces and a significantly longer stroke. Performance data of these actuators can be looked up at the individual homepages or in [8]. However, current in-field applications are mostly limited to the field of mobile machinery, where they have already been introduced in some product series on the market to directly control valves with flow rates of up to 100 l/min, see e.g. the LCV from Bucher Hydraulics [5]. In this case the actuators are used in combination with a pressure balance valve, which means that the differential pressure across the valve is always constant, limiting the maximum flow rate to the nominal flow rate chosen during the design process.

Even though the disadvantages of hydraulic pilot control, such as the sensitivity of the position regulation quality of pilot-operated valves to pressure fluctuations, contamination, and low temperatures, are particularly significant in the field of mobile machinery, it seems obvious to use these actuators also in industrial hydraulics to push the limits of direct pilot control above NS10. In contrast to applications with pressure balancing valves commonly used in the field of mobile machinery, the flow rates in industrial valves can be much greater than the nominal flow rate, as a pressure balancing valve does not control the pressure difference over the valve. While valves of NS10 in the standard market range have a minimum nominal flow rate of around 30 l/min and a maximum flow rate of 75 l/min (see **Figure 2**), the flow rate increases to around 100 l/min and 460 l/min, respectively, for the next larger NS16 valves (see **Figure 3**). Consequently, the flow rates controlled by NS10 valves are smaller compared to those already achieved in known mobile applications. For NS16 valves, on the other hand, although the nominal flow rates remain comparable, the maximum flow rate can exceed 100 l/min by four times.

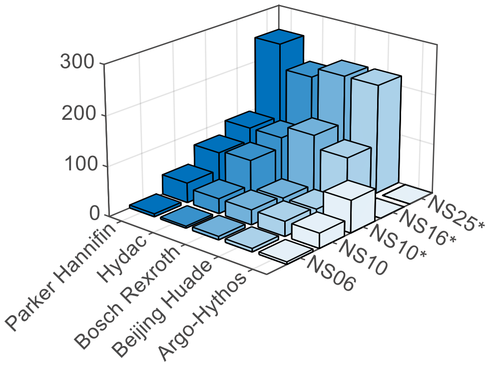

Figure 2: Nominal flow rate of proportional valves of different nominal sizes and manufacturers

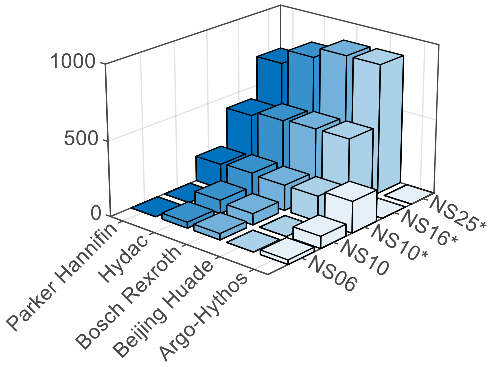

Figure 3: Maximum flow rate of proportional valves of different nominal sizes and manufacturers

In most cases, an increase in flow rate and valve size results in higher stroke and actuating force, unless the valve design has been specifically optimized to counteract these effects. For valves NS16, this typically results in forces and strokes that exceed the capabilities of conventional solenoids, which is why they are generally pilot-operated. Together with its industrial partner KMS Stoßdämpfer GmbH, ifas is currently working to demonstrate that the availability of previously presented actuators based on stepper or BLDC motors has opened up further potential for the direct control of larger valves in the field of industrial hydraulics. This is the first step towards shifting the application limit for direct control from NS10 to NS16 and making corresponding valves available on the market, thereby unlocking the associated potential for system optimization and performance enhancement.

This contribution not only aims to develop the initial step towards a directly controlled NS16 industrial valve but also employs systematic analysis to demonstrate how flow forces on spool valves can be reduced through appropriate geometric optimization. These findings can be applied to other valves from various manufacturers and in different sizes, facilitating a general evaluation of the feasibility of direct electromechanical control for larger valves using actuators based on stepper or BLDC motors.

2. New Direct Driven Proportional Valve NS16

A central aspect of the project was the development of an optimized NS16 hydraulic main stage, characterized by low operating forces. To this end, the first step was to develop a functional hydraulic main stage with a nominal flow rate of 125 l/min and a maximum flow rate of 400 l/min achieved at a pressure difference of max 70 bar over the metering notch. To keep the radial flow forces as low as possible and at the same time enable easy adjustment of the internal geometry, the valve was designed as a sleeve valve. This allows systematic investigation of different geometries for the spool and sleeve to demonstrate the potential for reducing flow forces. A cross-sectional view of the prototype is shown in **Figure 4**.

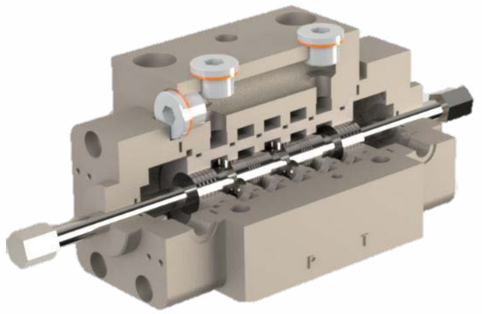

Figure 4: CAD of the developed direct driven main stage

2.1. Force Requirements

Since the valve cannot be actuated if the generable forces are insufficient, achieving an appropriate actuating force is a fundamental requirement for the implementation of direct electromechanical actuation. To determine the necessary actuating force, all forces acting on the spool must be analyzed. **Figure 5** shows a corresponding spool with all the forces acting on it. These are usually the spring forces F_C, friction forces F_R, flow forces F_{Flow}, and the actuating force F_{Act}.

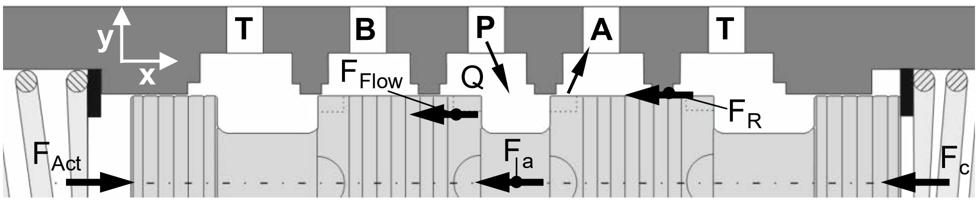

Figure 5: Forces acting on the slide of a globe valve according to [21]–[23]

Within the illustration, the spool is assumed to be deflected in the positive x-direction, with positive velocity and acceleration. Friction (F_R), inertial forces (F_a) and spring forces (F_C) therefore act in the negative x-direction, and the actuating force (F_{Act}) exceeds the sum of all these opposing forces. Since this is a standard design without any flow force compensation geometries, it can be assumed that the flow forces (F_{Flow}) act in the closing direction and thus in the negative x-direction. In this case, the force balance on the spool can be formulated according to **Equation 2.1**.

$$F_{Act} = F_a + F_C + F_R + F_{Flow} \tag{2.1}$$

To keep the required force as low as possible, all opposing forces must be minimized. However, each one can only be reduced to a limited extent due to their causes or functions.

2.2. *Inertia Forces*

Since inertial forces are defined by mass m and acceleration $\ddot{x}$ for a given acceleration profile, they can only be reduced by decreasing the mass. However, this is only possible to a limited extent, as both the shape and material of the spool cannot be chosen arbitrarily. For the valve considered in this contribution, the inertia force was estimated assuming that the spool must travel the full stroke of 7.5 mm within 50 ms, accelerating until the midpoint of the stroke followed by a subsequent constant deceleration. With a mass of 300 g this leads to an inertia force of 18 N.

2.3. *Frictional Forces*

In the context of pilot-operated valves, friction forces typically refer to those forces acting between the spool and the housing or sleeve. According to common models, these forces consist of a Newtonian and a Coulombian component. They always oppose the direction of movement and thus have a damping effect on the valve spool motion. The choice of material, the fit between the spool and the sleeve, and the radial flow forces influences friction. A careful trade-off must be made in terms of this fit. It must be tight enough to prevent excessive leakage but not so tight that frictional forces become too large.

2.4. *Flow Forces*

Flow forces are generally defined as the sum of the forces caused by the flow of fluid. These are usually forces resulting from uneven pressure distribution, viscous friction forces, and inertia and acceleration forces of the fluid [24], [25]. The law of conservation of momentum is usually used to derive a usable equation**.** Thereby, a control volume defined in the flow area between the spool, and the housing is used to calculate the flow force, see **Figure 6**. At the selected control volume, the flow Q enters the control volume at the P port at a velocity $\vec{v}_1$ at an angle of ε_1 and leaves the system at a velocity $\vec{v}_2$ at an angle of ε_2 at port A.

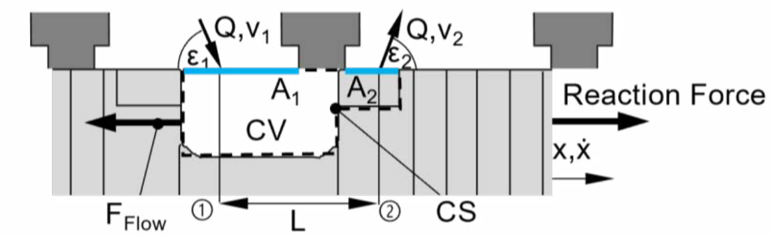

Figure 6: Derivation F_{Flow} using the law of conservation of momentum [22], [26]–[29]

Using Reynolds' transport theorem, the equation for the flow forces can be written according to **Equation 2.2**.

$$\sum \vec{F} = \frac{d}{dt}\left(\int_{CV} (\rho \cdot \vec{v}) dV\right) + \int_{CS} \rho \cdot \vec{v}(\vec{v} \cdot \vec{n}) dA \tag{2.2}$$

The flow forces are derived analytically from the temporal derivative of the integral of density ρ and the velocity vector $\vec{v}$ over the volume V of the control volume CV, added to the integral of the product of density ρ, velocity vector $\vec{v}$ and the scalar product of velocity vector $\vec{v}$ with direction vector $\vec{n}$ integrated over the area A of the whole control surface (CS). The first part of the equation describes the unsteady flow force and thus forces related to the inertia and acceleration of the fluid, while the second term describes the steady state flow forces. While steady state axial flow forces have been well researched today, the number of studies dealing with the unsteady flow force is considerably lower. However, these studies show that the unsteady flow force for slow and moderately switching valves is considerably lower than the steady state flow forces. The assumption of quasi-steady state that is usually made, therefore, can generally be considered valid [30].

2.4.1. Axial Flow Forces

Using the orifice equation and assuming constant fluid density, ideal rotational symmetry, sharp metering edges, and a negligible clearance between the spool and the sleeve, the equation for the steady-state axial flow force for one metering edge can be expressed as follows [27], [31].

$$\mathrm{F}_{Flow,\mathrm{axial,stat}} = 2\alpha_{\mathrm{D}}^{2} \cdot \pi \cdot \mathrm{d} \cdot \mathrm{x} \cdot \Delta p \cdot \frac{\cos(\varepsilon_1)}{\sin(\varepsilon_1)} \tag{2.3}$$

While measuring the axial flow forces, frictional forces typically superimpose on them. As a result, plotting the measured force against position usually produces a hysteresis loop (see **Figure 7**).

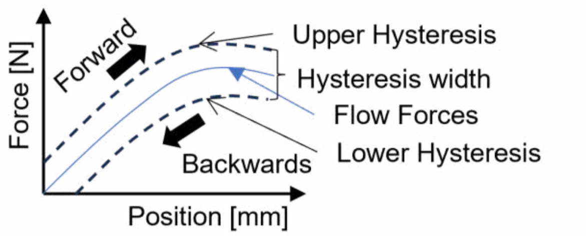

Figure 7: Illustration of measured forces: Hysteresis and flow forces

Assuming the frictional forces are equal in both the opening and closing directions, the axial flow forces are centered within the hysteresis, with half the width of the hysteresis corresponding to the frictional force. [21], [22], [27], [32]

2.4.2. Radial Flow Forces

For the radial flow forces, Equation 2.2 must be integrated over the circumference of the spool. With an ideally rotationally symmetrical geometry and an ideally rotationally symmetrical flow, these forces would completely compensate each other, resulting in a total net force of 0 N. In reality, however, perfect rotational symmetry of geometry and flow profile is rarely achieved, so that radial flow forces usually still occur. An increase in the nominal forces acting on the spool results in higher Coulomb friction forces; consequently, variations in the hysteresis width may reflect changes in the radial flow force [32].

2.4.3. Spring Forces

For 4/3-way valves, the rest position defined by the springs can be either one of the two switched positions (A or B) or the center position (0). In Figure 5, a valve with a blocked center position is shown, in which both springs push the spool into the center position. Since a secure rest position must always be ensured and reached within a specified time, the springs must be designed accordingly. In the case of pilot-controlled valves, the required actuating force usually does not need to be considered, as forces in the kN range can typically be achieved. Therefore, in proportional valves, springs are chosen to have high stiffness in order to achieve high accuracy within the control loop [33].

However, stepper motors are inherently capable of moving to a defined position. Even when operated in a closed-loop position control system via the motor controller to improve accuracy, spring stiffness has only a minor influence on position control. Given the limited forces available from electromechanical actuators, it is therefore advisable to design the spring with the lowest possible stiffness while selecting the highest possible preload force. Selecting a suitable spring within the available installation space presents a separate optimization problem. Nevertheless, to achieve the highest possible spring force and thus minimize return time while considering the limited actuation forces, all other opposing forces must be kept as low as possible, which is why flow forces need to be reduced.

3. PRINCIPLES FOR FLOW FORCE REDUCTION

The reduction of flow forces by optimizing spool geometries is a widely researched topic and is regularly discussed in the technical literature [10], [13], [15]–[17], [34]–[38]. However, most studies focus on servovalves, with optimizations that are difficult to adapt to proportional valves with metering notches. Therefore, this contribution investigates geometric optimization methods for reducing flow forces that can be applied to proportional valves with metering notches. Based on theoretical, analytical, and literature-based considerations [11], [12], [14], [16], [35], [37], [39]–[41], possible geometric optimizations for the spool and sleeve were identified. Their potential to enable direct actuation by electromechanical actuators through the reduction of flow forces is investigated in a systematic study on the NS16 main stage developed as part of this work. For the evaluation of this potential, a non-optimized proportional valve, shown in **Figure 8**, serves as the reference. The geometric optimizations investigated are illustrated in **Figure 9**.

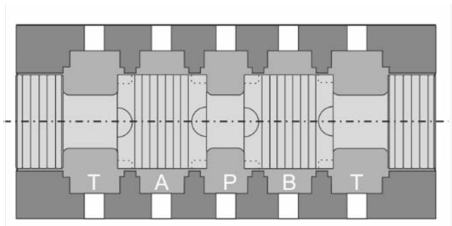

Figure 8: Spool without features

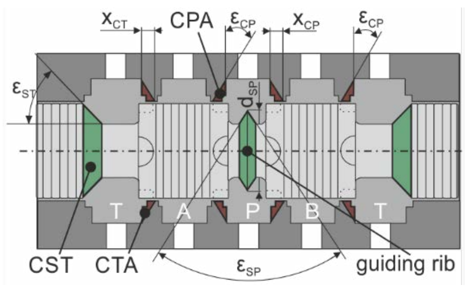

Figure 9: Spool with features

Compared to the non-optimized geometry, Figure 9 shows areas in green where additional material needs to be added, and areas in orange where material must be removed. For the sleeve, adding a chamfer to the partition between the valve chambers was identified as a promising way to achieve sufficient flow guidance and thereby reduce flow forces. Two geometric parameters are required to fully define this chamfer the angle ε and the chamfer length x. At the Port P, it is referred to as chamfer CPA and defined by the parameters x_{CP} and ε_{CP}. At the Port T, it is referred to as chamfer CTA and is defined by x_{CT} and ε_{CT}. For the spool, a centrally located guiding rib at the geometric center and an additional chamfer at the outer shoulder of the T-Port were identified as possible optimizations for reducing flow forces. The guiding rib can be fully described by d_{SP} and ε_{SP}, while the chamfer CST is characterized by the angle ε_{ST}. Whereas the guiding rib and chamfer CST are established features used in prior studies and industrial applications to reduce flow forces (see [11], [12], [14], [16], [35], [37], [40], [41]), the sleeve chamfers represent an optimization derived from theoretical considerations.

In order to achieve the most efficient reduction in flow forces based on the reference geometry, the influence of the geometric features was analyzed in a three-step process consisting of two simulation steps carried out with ANSYS Fluent CFD-Software and one experimental step. The first step involved a statistical analysis whereby a parameterized CAD model was imported into the simulation software, and simulation points were generated and solved using an optimally space-filling design. Response surfaces were then derived from these simulations to assess the influence of each feature. Subsequently, each feature was simulated individually to determine suitable parameters. As a result, four valve geometries incorporating the identified measures were manufactured and tested experimentally.

To keep the simulation effort manageable, it was important to minimize the computational domain in the CFD simulations. Therefore, the valve was divided into two separate models, each examined individually. The first model, system P, includes the P-port and one working port (A), allowing investigation of flow from P to A. The second model, system T, includes the other working port (B) and the T-port, enabling analysis of flow from B to T. This division made it possible to specifically study both flow scenarios and to investigate the features separately, while also reducing computational complexity.

3.1. Validation of CFD Simulation

To validate the CFD simulations, the reference geometry was first manufactured and measured. The ifas has a measuring device and a test bench available for this purpose. The measuring device consists out of a stepper motor, whose rotational motion is converted into linear motion via a threaded rod and nut assembly with a pitch of 3 mm. A force sensor is integrated into the connection between the actuation unit and the spool to measure the forces which are acting on the spool. To minimize the influence of transverse forces on the measurement, a combination of clevis and head joints was implemented. Additionally, prior to the measurement, the device was carefully aligned with the valve spool. Therefore, the actuation mechanism was moved over the full stroke to ensure that resulting friction forces were as low as possible. Additionally, a position sensor was incorporated to monitor the position of the spool. A similar actuation device also designed by ifas has been described in [42].

The circuit diagram of the test rig can be found in [43]–[45]. While this configuration enables measurement of the forces acting on the spool during flow from the pressure port

(P) to either of the working ports (A or B), as well as during overall flow through the valve (PABT/PBAT), it does not permit individual measurement of flow from either working port (A or B) to the tank port (T). Consequently, separate analysis of the return flow paths (AT or BT) is not possible.

For the reference geometry, the target flow rate of 400 l/min was achieved at a pressure difference of 60 bar, while at a pressure difference of 5 bar, a flow rate of 125 l/min was achieved. In line with theoretical expectations, an increase in pressure difference resulted in a corresponding increase in flow force. Consequently, operation at a pressure difference of 60 bar led to the highest observed flow forces within the pressure range (5 – 60 bar). The results of the simulations and measurements for a pressure difference of 60 bar for the system P (Flow from P to A) of the reference geometry are shown in **Figure 10**. Within the simulation the mesh consists of around 13 Mio Cells with local refinement within relevant areas like the metering notches or the inlet and outlet. The average orthogonality was 0.9662 and the skewness 0.03381.

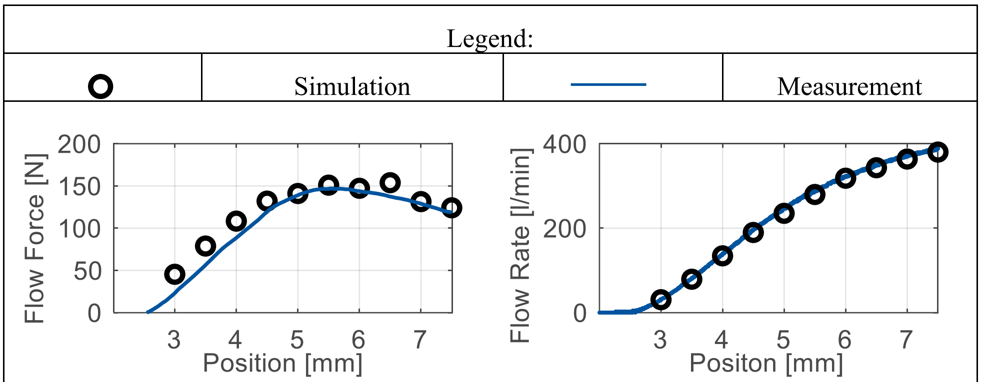

Figure 10: Comparison Simulation Measurement for Flow Rate and Flow Force

As can be seen in the graphs, the simulation results correspond very well with the measurement data. The CFD simulation can therefore be used to generate reliable results in terms of both flow rate and flow forces for the considered system P of the reference geometry.

3.2. Statistical Evaluation of Principles (CFD-Simulation)

The following **Figure 11** to Figure 14 show examples of the response surfaces for the guiding rib feature, illustrating the influence of the parameters diameter d_{SP} and angle ε_{SP}. Since both the flow force and the flow rate must be considered over the entire range of spool positions x, the visualizations are presented as three-dimensional characteristic maps. The resulting flow force F_{Flow} and flow rate Q are plotted on the Z-axis, spool position x on the Y-axis, and the value of each geometric feature under investigation (e.g., d_{SP} and ε_{SP}) on the X-axis. This form of representation enables a detailed analysis of how spool position and geometric features interact to affect flow force and flow rate.

As shown in **Figure 11**, the guiding rib is particularly effective for large valve openings (X) and large diameters (d_{SP}). For diameters greater than 20 mm, even negative forces are achievable, which means that the system is overcompensated and the flow force is acting in opening direction. However, selecting a large diameter d_{SP}, may negatively affect the flow rate characteristic curve. This can be seen in **Figure 12**, where the flow rate drops for diameters larger than 20 mm. By appropriately selecting the diameter d_{SP}, it is possible to reduce the flow force without adversely impacting the flow rate characteristic for example with diameters of maximum 20 mm. **Figure 13** and Figure 14 show the response surfaces for the angle ε_{SP} of the guiding rib. As can be seen the angle ε_{SP} of the guiding rib has a relatively minor influence on the flow force. Angles around 100° result in a maximum flow force, whereas both smaller and larger angles have a slightly positive effect by reducing the flow force. At the same time, the impact of angle ε_{SP} on the flow rate characteristics is very small.

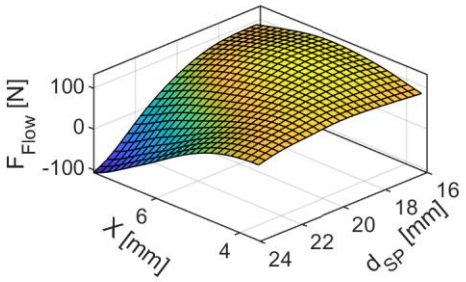

Figure 11:Response Surface F_{Flow}-X-d_{SP}

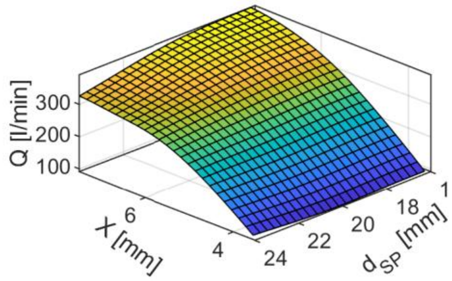

Figure 12: Response Surface Q-X-d_{SP}

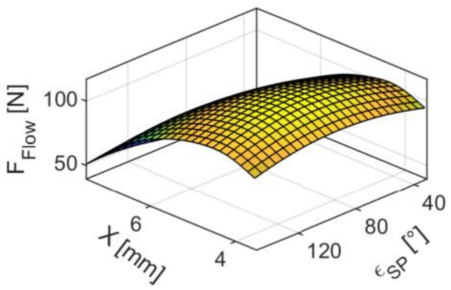

Figure 13: Response Surface F_{Flow}-X-ε_{SP}

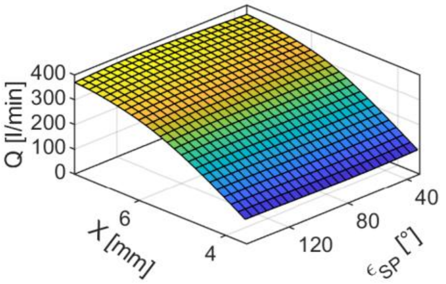

Figure 14: Response Surface Q-X-ε_{SP}

3.3. Simulation of the various concepts

In statistical analysis, the influence of individual features can be evaluated quickly and efficiently. However, assessing combined effects is significantly more complex. After it was proven that all features can have a positive effect, their influence was systematically analyzed in a second step to identify optimal design parameters. As the key objective of this investigation was to identify the potential of each individual design feature for reducing flow forces, a targeted exploration of the design features was preferred over deriving a statistical model in the following. This approach enables a direct and transparent assessment of each feature's contribution to flow force reduction. Initial parameters for each feature were selected based on the prior results, and then individual parameters were systematically varied to identify suitable values for each feature.

From the results, two promising configurations for both the spool and the sleeve were selected, each with and without optimization features. This allowed four different valve configurations to be formed. $Spool_{Ref}$-$Sleeve_{Ref}$ without any feature, $Spool_{Opt}$-$Sleeve_{Ref}$ with features in the spool, $Spool_{Ref}$-$Sleeve_{Opt}$ with features in the sleeve and $Spool_{Opt}$-$Sleeve_{Opt}$ with features applied to both the spool and the sleeve. By the different combinations, the effectiveness of each feature could be examined separately and in combination. The selected geometric values were as follows. The angles ε_{SP}, ε_{ST}, ε_{CP} and ε_{CT} were set to 45°, the removal depths X_{CP} and X_{CT} to 5 mm and the diameter d_{SP} to 22 mm.

Simulation results for these geometries at a pressure level of 60 bar are presented in **Figure 15** and **Figure 16** (system P) and **Figure 17** and **Figure 18** (system T). The simulation results of system P show that all features are effective in reducing flow forces. However, the guiding rib feature can negatively affect the flow rate characteristic, as the flow rate decreases for strokes greater than 5 mm. This negative effect can be avoided when the guiding rib is combined with the chamfer in the sleeve.

For the system T, it can also be concluded that all features have a positive effect, with no negative impact on the flow rate characteristic curve. Notably, in the $Spool_{Opt}$-$Sleeve_{Ref}$ and $Spool_{Opt}$-$Sleeve_{Opt}$ configurations, the chamfer at the spool leads to an opposing flow force for strokes greater than 4 mm respectively 6.5 mm, resulting in overcompensation.

Legend:			
	$Spool_{Ref}$-$Sleeve_{Ref}$		$Spool_{Opt}$-$Sleeve_{Ref}$
	$Spool_{Ref}$-$Sleeve_{Opt}$		$Spool_{Opt}$-$Sleeve_{Opt}$

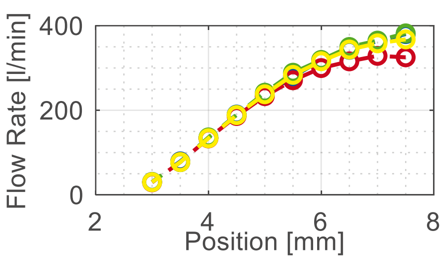

Figure 15: Simulation Results Flow Rate System P

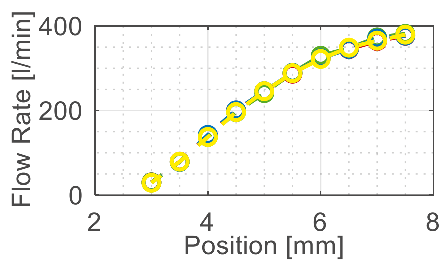

Figure 16: Simulation Results Flow Rate System T

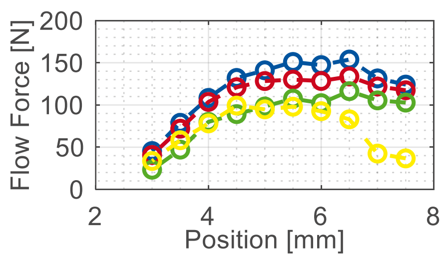

Figure 17: Simulation Results Flow Forces System P

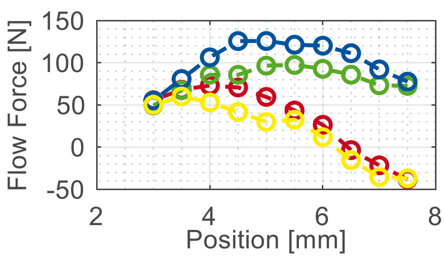

Figure 18: Simulation Results Flow Forces System T

4. EXPERIMENTAL EVALUATION OF COMBINED PRINCIPLES

Once the effectiveness of the features had been identified through simulations, all versions were evaluated experimentally. To this end, the two spool and sleeve variants were manufactured and measured in their respective combinations. Measurements were conducted for system P, where flow occurs from P to A, as well as for the combined system PT, where flow occurs from P to B and from A to T, using the available test bench. Unfortunately, it was not possible to measure system T separately due to limitations of the existing test rig. Therefore, only the simulations result of system A can directly be compared with measurement data. The simulations result of system T can only be analyzed using the measurements of system P and PT, as by comparison between both systems the effectiveness of the features of system T can be identified. The measurement results are shown in **Figure 19** to **Figure 22.**

Legend:			
	$Spool_{Ref}$-$Sleeve_{Ref}$		$Spool_{Opt}$-$Sleeve_{Ref}$
	$Spool_{Ref}$-$Sleeve_{Opt}$		$Spool_{Opt}$-$Sleeve_{Opt}$

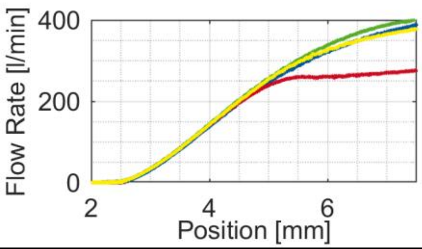

Figure 19: Flow Rate System P

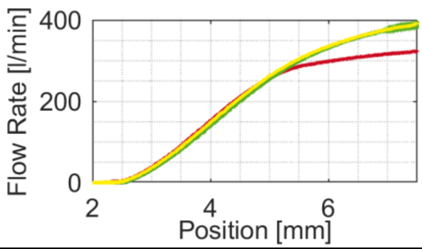

Figure 20: Flow Rate System PT

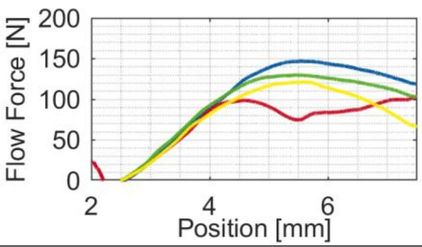

Figure 21: Flow Forces System P

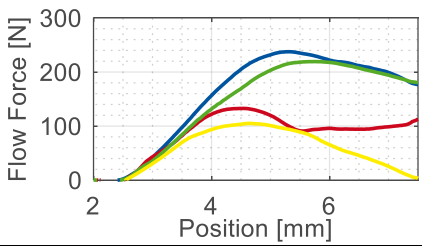

Figure 22: Flow Force System PT

The measurement data show that the configuration without optimization features exhibits the highest flow forces, and that applying the features produces the expected effects, as anticipated from the CFD simulations. Implementing the features on the spool alone leads to a reduction in flow force; however, this is accompanied by a decrease in flow rate, as assumed from the simulation whereby the impact is underestimated within the simulation. Within simulations conducted at a pressure difference of 70 bar, the effect was considerably more pronounced. It remains questionable whether the observed reduction in flow force is genuinely due to the optimization or simply a result of the lower flow rate. Optimizations to the sleeve show a positive effect, with a reduction of 12 %, although this is significantly less than predicted by simulation. The same applies to the combination of both measures. In this case, flow forces were reduced by 18 %, indicating a clear positive effect but still falling short of the optimistic simulation results. When only the system P is flowed through, the proposed features lead to a reduction in flow force of 18 %. When both PB and AT are evenly flowed through, an even greater reduction of 65 % is achieved.

Since simulations appear to overestimate the potential of sleeve optimization, further analysis is required to determine the reason for this discrepancy and improve the simulation models. In this study, CFD was employed as a design tool to efficiently investigate the effects of various geometric features on flow forces. By systematically screening a large number of design variants through simulation, it was possible to identify promising designs for experimental validation without having to manufacture each individual parameter set. This approach allowed for a significant reduction in the number of required measurements and enabled efficient identification of improved geometries. Consequently, further refinement of the simulation models be desirable for future valve improvements, however such optimization of the simulation model lies beyond the scope of this contribution

5. SUMMARY AND OUTLOOK

Over the past ten years, new actuators based on stepper and BLDC motors have been tested for use in mobile hydraulics and have also been introduced to the market in some products. Compared to conventional solenoids, these actuators are characterized by higher forces and strokes, making them a viable alternative to hydraulic pilot control. Direct control offers several advantages over hydraulic pilot control, especially in mobile machines where highly fluctuating loads, operation with cold fluid during startup, and heavy fluid contamination are common conditions. Due to their increased forces and strokes, these actuators also have potential applications in stationary hydraulics. In this context, they could help shift the system limit for direct control from NS10 to NS16.

However, the maximum possible flow rates in stationary hydraulics are considerably greater than those in mobile applications, which increases demands on the actuator. While spring forces should be minimized overall, maximizing them within the limits of the actuator's maximum capacity helps to minimize reset times and enhance system safety. Therefore, reducing flow forces is essential.

Within the scope of this contribution, various flow force compensation design features that can be implemented on conventional proportional spools and sleeves/housings were identified, analyzed and investigated by simulations and measurements for their potential to reduce flow forces. Overall, flow forces could be reduced by 18 % percent compared to a reference spool without optimization measures. In particular, the chamfer in the sleeve (ε_{CP}, x_{CP}) and the additional angle ε_{ST} on the spool demonstrated high potential for reducing flow forces while having only a minor impact on the flow rate characteristic curve. The addition of a guiding rib also resulted in a reduction in flow forces, however, if not correctly designed, it can negatively affect the flow rate characteristic curve.

The reduction in flow forces achieved helps to keep the total required actuating force as low as possible. Depending on the selected spring, the necessary actuating forces may be matched to the maximum output of modern actuators. Therefore, reducing flow force is a decisive step toward enabling direct electromechanical control of large valves.

6. REFERENCES

[1] Max-Eyth-Gesellschaft für Agrartechnik: 'Landtechnik 1995 - Tagung Braunschweig, 12. und 13. Oktober 1995', VDI-Berichte, VDI-Verl., Düsseldorf, 1995.

[2] Manfred Becker: 'Schrittmotoren als Aktuator für Hydraulik-Wegeventile'.

[3] Schwander, P., Flückiger, M. 'Aktuator für Schieberventile in der mobilen Hydraulik', ATZoffhighway, Vol. 7, Nr. 3, pp. 70–77, 2014. DOI: 10.1365/s35746-014-0194-3.

[4] Lux, J., Habegger, C. 'New generation of intelligent electromechanical valve actuation', 11TH INTERNATIONAL FLUID POWER CONFERENCE, pp. 394–402, 2018.

[5] Bucher Hydraulics: 'Proportionalwegeventile - Baureihe LCV', https://www.bucherhydraulics.com/datacat/files/Katalog/Ventile/Zwischenplattenventile_Sandwichventile/LCV/LCV_100-P-000161-de.pdf, 2022.

[6] Sonceboz: 'Elektromechanische Ventilantriebe ergänzen die Hydraulik'.

[7] Norbert Menden: 'Punktgenau in allen Klimazonen - Ventil mit Can-Aktuator für mobile Anwendungen', https://www.fluid.de/abo/heftarchiv/ausgabendetail/fluid-01-02-2018.html, 2018.

[8] Ermert, M. 'Electromechanical actuator concept for the controlled and direct actuation of a hydraulic main stage', 10TH INTERNATIONAL FLUID POWER CONFERENCE, pp. 503–513, 2016.

[9] Sonceboz: 'SMART LINEAR ACTUATOR', https://sonceboz.com/product/smart-linear-actuator/.

[10] Schuster, G. 'CFD-gestützte Maßnahmen zur Reduktion von Strömungskraft und Kavitation am Beispiel eines hydraulischen Schaltventils', Reihe Fluidtechnik D, Shaker, Aachen, 2005.

[11] Tamburrano, P., Plummer, A. R. et al. 'A Review of Direct Drive Proportional Electrohydraulic Spool Valves: Industrial State-of-the-Art and Research Advancements', Journal of Dynamic Systems, Measurement, and Control, Vol. 141, Nr. 2, 2019. DOI: 10.1115/1.4041063.

[12] Amirante, R., Moscatelli, P. G., Catalano, L. A. 'Evaluation of the flow forces on a direct (single stage) proportional valve by means of a computational fluid dynamic analysis', Energy Conversion and Management, Vol. 48, Nr. 3, pp. 942–953, 2007. DOI: 10.1016/j.enconman.2006.08.024.

[13] Jackson, R. S., Belger, M. M. et al. 'CFD SIMULATION AND EXPERIMENTAL INVESTIGATION OF STEADY STATE FLOW FORCE REDUCTION IN A HYDRAULIC SPOOL VALVE WITH MACHINED BACK ANGLES', BATH/AMSE 2017 Symposium on Fluid Power and Motion Control, 2017.

[14] Chen, L., Zhang, C. et al. 'Simulation and experimental research on steady flow force compensation for a servo proportional valve', Flow Measurement and Instrumentation, Vol. 94, pp. 102457, 2023. DOI: 10.1016/j.flowmeasinst.2023.102457.

[15] Ding, X., Li, R. et al. 'Study on flow force compensation characteristics and optimization design of jet guiding groove', Flow Measurement and Instrumentation, Vol. 86, pp. 102194, 2022. DOI: 10.1016/j.flowmeasinst.2022.102194.

[16] Gui, S., Zhang, S. et al. 'Fluid-dynamic analysis and multi-objective design optimization of piezoelectric servo valves', Flow Measurement and Instrumentation, Vol. 85, pp. 102157, 2022. DOI: 10.1016/j.flowmeasinst.2022.102157.

[17] Li, R., Wang, Z. et al. 'Design and optimization of hydraulic slide valve spool structure based on steady state flow force', Flow Measurement and Instrumentation, Vol. 96, pp. 102568, 2024. DOI: 10.1016/j.flowmeasinst.2024.102568.

[18] Zhou, D., Jin, B. et al. 'Modeling, simulation and optimization of a pilot-operated threaded cartridge proportional relief valve', Flow Measurement and Instrumentation, Vol. 107, pp. 103071, 2026. DOI: 10.1016/j.flowmeasinst.2025.103071.

[19] Yang, M., Lian, K. et al. 'Simulation analysis and optimization of pilot type electro-hydraulic proportional directional valve based on multi field coupling', Flow Measurement and Instrumentation, Vol. 100, pp. 102726, 2024. DOI: 10.1016/j.flowmeasinst.2024.102726.

[20] Elsaed, E., Linjama, M. 'A Review of Pilot-operated Hydraulic Valves – Development, Challenges, and a Comparative Study', International Journal of Fluid Power, 2023. DOI: 10.13052/ijfp1439-9776.2443.

[21] Backé, W., Tatar, H. 'Untersuchung des Einflusses von Störkräften auf den Schaltvorgang bei Wegeventilen der Hydraulik', Forschungsberichte des Landes Nordrhein-Westfalen, Westdt. Verl., Opladen, 1975.

[22] Bordovsky, P. 'Evaluation of steady-state flow forces in spool valves - = Evaluierung stationärer Strömungskräfte in Schieberventilen', Reihe Fluidtechnik. D, [1. Auflage], Shaker Verlag, Düren, 2019.

[23] Schrank, K., Murrenhoff, H. 'Beschreibung der Strömungskraft in Längsschieberventilen mittel Impulserhaltung', O+P Journal, Nr. 4, pp. 4–15, 2013.

[24] Bordovsky, P., Murrenhoff, H. 'Investigation of steady-state flow forces in spool valves of different geometries and at different oil temperatures with the help of measurements and cfd simulations', BATH/AMSE 2016 Symposium on Fluid Power and Motion Control, 2016.

[25] Bordovsky, P., Schmitz, K., Murrenhoff, H. 'CFD Simulation and Measurement of Flow Forces Acting on a Spool Valve', 10TH INTERNATIONAL FLUID POWER CONFERENCE, pp. 473–484, 2016.

[26] Herakovič, N., Duhovnik, J., Šimic, M. 'CFD simulation of flow force reduction in hydraulic valves', Tehnički vjesnik - Technical Gazette, Vol. 22, Nr. 2, pp. 453–463, 2015. DOI: 10.17559/tv-20141128090939.

[27] Bordosky, p., Murrenhoff, H. 'VALIDATION OF AN ENHANCED MODEL OF STEADY-STATE FLOW FORCES FOR SPOOL VALVES', The 10th JFPS International Symposium on Fluid Power, 2017.

[28] Bordovsky, P., Murrenhoff, H. 'Analysis of Flow Angles and Flow Velocities in Spool Valves for the Calculation of Steady-State Flow Forces', The 15th Scandinavian International Conference on Fluid Power, pp. 371–379, 2017. DOI: 10.3384/ecp17144371.

[29] Ye, Y., Yin, C.-B. et al. 'Effects of groove shape of notch on the flow characteristics of spool valve', Energy Conversion and Management, Vol. 86, pp. 1091–1101, 2014. DOI: 10.1016/j.enconman.2014.06.081.

[30] Del Vescovo, G., Lippolis, A. 'A review analysis of unsteady forces in hydraulic valves'.

[31] Schmitz, K., Murrenhoff, H. 'Grundlagen der Fluidtechnik', Reihe Fluidtechnik. U, Vollständig neu bearbeitete Auflage, 2018.

[32] Hucko, S., Vonderbank, T., Schmitz, K. 'Investigation of Frictional Forces in Hydraulic Spool Valves and Their Effect on the Estimation of Axial Flow Forces', ASME/BATH 2023 Symposium on Fluid Power and Motion Control, 2023. DOI: 10.1115/FPMC2023-111904.

[33] Lisowski, E., Filo, G., Rajda, J. 'Pressure compensation using flow forces in a multi-section proportional directional control valve', Energy Conversion and Management, Vol. 103, pp. 1052–1064, 2015. DOI: 10.1016/j.enconman.2015.07.038.

[34] Ristic, M. 'Dreidimensionale Strömungsberechnungen zur Optimierung von Hydraulikventilen bezüglich der stationären Strömungskräfte', Reihe Fluidtechnik D, Shaker, Aachen, 2000.

[35] Amirante, R., Distaso, E., Tamburrano, P. 'Sliding spool design for reducing the actuation forces in direct operated proportional directional valves: Experimental validation', Energy Conversion and Management, Vol. 119, pp. 399–410, 2016. DOI: 10.1016/j.enconman.2016.04.068.

[36] Borghi, M., Milani, M., Paoluzzi, R. 'Stationary Axial Flow Force Analysis on Compensated Spool Valves', International Journal of Fluid Power, Vol. 1, Nr. 1, pp. 17–25, 2000. DOI: 10.1080/14399776.2000.10781079.

[37] Herakovič, N. 'Flow-force analysis in a hydraulic sliding-spool valve', Strojarstvo Casopis Za Teoriju I Praksu U Strojarstvu, Vol. 51, pp. 555–564, 2009.

[38] Bordovsky, P., Schmitz, K., Murrenhoff, H. 'Anwendung der statistischen Versuchsplanung zur Parametidentifiaktion für Strömungskraftberechungen', 2018.

[39] Borghi, M., Milani, M. 'Influence of Notch Shape and Number of Notches on the Metering Characteristics of Hydraulic Spool Valves', International Journal of Fluid Power, Vol. 6, pp. 5–18, 2005. DOI: 10.1080/14399776.2005.10781216.

[40] C. Qianpeng, J. Hong et al. 'Proposal for Optimization of Spool Valve Flow Force Based on the MATLAB-AMESim-FLUENT Joint Simulation Method', IEEE Access, Vol. 6, pp. 33148–33158, 2018. DOI: 10.1109/ACCESS.2018.2846589.

[41] Lugowski, J. 'FLOW FORCE IN A HYDRAULIC SPOOL VALVE'.

[42] Aengenheister, S., Liu, C. et al. 'Functional proof of a flat slide valve as a 4/3-way proportional valve', 12TH INTERNATIONAL FLUID POWER CONFERENCE, pp. 163–170, 2020. DOI: 10.25368/2020.24.

[43] Vonderbank, T., Laßl Chavez, P. M., Schmitz, K. 'Direct Actuation of Large Sized Valves by a Hydraulically Relieved Electromechanical Actuation System', International Journal of Fluid Power, 2021. DOI: 10.13052/ijfp1439-9776.2312.

[44] Vonderbank, T., Schmitz, K. 'ELECTROMECHANICAL ACTUATOR FOR LARGE SIZED DIRECTIONAL CONTROL VALVES', 10th International Conference on Fluid Power Transmission and Control, ICFP, pp. 312–317.

[45] Vonderbank, T., Laßl Chavez, P. M., Schmitz, K. 'Novel hydraulically relieved electromechanical direct actuation system for large scale switching valves', The 17th Scandinavian International Conference on Fluid Power, pp. 173–185.

Biographies

Tobias Vonderbank received the Bachelor of Engineering from Hochschule Niederrhein University for Applied Sciences in 2016 and the Master of Science from RWTH Aachen University in 2018. He is currently working as a Research Associate at the Institute for Fluid Power Drives and Systems, RWTH Aachen University. His research areas are Fluid Power, valves and electromechanical valve actuation systems.

Prof. Katharina Schmitz studied mechanical and chemical engineering at RWTH Aachen University and Carnegie Mellon University, Pittsburgh (USA) and graduated 2015 as Dr.-Ing. at RWTH Aachen University. Since 2018, she is full professor at RWTH Aachen University and director of the Institute for Fluid Power Drives and Systems (ifas). In addition, she is Vice Dean of the Faculty for Mechanical Engineering at RWTH Aachen, a position she holds since 2020. Prof. Schmitz's awards and honors include several best paper awards and 2023 IMechE Joseph Bramah Medal award.